Maintaining intestinal structural integrity is a potential protective mechanism against inflammation in goose fatty liver

Wang Gu,[*] Kang Wen,[*] Chunchi Yan,[*] Shuo Li,[*] Tongjun Liu,[*] Cheng Xu,[*] Long Liu,[*] Minmeng Zhao,[*] Jun Zhang,[*] Tuoyu Geng,[*,†,1] and Daoqing Gong[*,†,1]

[*]*College of Animal Science and Technology, Yangzhou University, Yangzhou, Jiangsu Province 225009, P. R. China; and* [†]*Joint International Research Laboratory of Agriculture and Agri-Product Safety of the Ministry of Education of China, Yangzhou University, Yangzhou, Jiangsu Province 225009, P. R. China*

ABSTRACT Overfeeding causes severe steatosis but not inflammation in goose liver, suggesting existence of protective components. Previous studies have shown that some intestinal microbes and their metabolites damage intestinal structural integrity and function, thus causing inflammation in the development of human and mouse nonalcoholic fatty liver disease. Therefore, this study hypothesizes that intestinal structural integrity of goose is maintained during overfeeding, which may provide goose fatty liver a protective mechanism against inflammation. To test this hypothesis, 48 seventy-day-old healthy Landes male geese were overfed (as overfeeding group) or normally fed (as control group). Blood and intestine (jejunum, ileum, and cecum) samples were harvested on the 12th and 24th d of overfeeding. Data showed that goose fatty liver was successfully induced by 24 d of overfeeding. Hematoxylin-eosin staining analysis indicated that the arrangement of villi and crypts in the intestine was orderly, and the intestinal structure was intact with no pathological symptoms in the 2 groups. Enzyme-linked immunosorbent assay and quantitative PCR analysis indicated no significant differences in the expression of tight junction and inflammation-related genes as well as plasma lipopolysaccharide concentration between the groups. Ileal hypertrophy and cecal atrophy were observed in the overfed vs. control geese, probably because of change of sphingolipid metabolism. Activation of apoptotic pathway may help cecum avoid necrosis-induced inflammation. In conclusion, healthy and intact intestine provides a layer of protection for goose fatty liver against inflammation. Sphingolipid metabolism may be involved in the adaptation of ileum and cecum to overfeeding. The hypertrophy of ileum makes it an important contributor to the development of goose fatty liver. The atrophy and decline in the function of cecum may be caused by apoptosis induced by overfeeding.

Key words: goose fatty liver, intestinal barrier, inflammation, apoptosis, sphingolipid metabolism

2020 Poultry Science 99:5297–5307
https://doi.org/10.1016/j.psj.2020.08.052

INTRODUCTION

Goose fatty liver (or *foie gras*), as a high-end food rich in nutrients, is produced by artificial overfeeding. It contains about 60% of fat, weighing around 800 g (Hermier et al., 1994). Based on the criterion of hepatic steatosis or fatty liver, that is, fatty liver occurs when fat content exceeds 5% of liver weight (Sanyal et al., 2011), goose fatty liver is usually in the state of severe steatosis. A lot heavier than normal liver and light yellow color are the successful signs of goose fatty liver. The great capacity of goose liver for fat deposition may be originated from the adaptation of their ancestors to long-distance migration (Hermier, 1997). Despite severe steatosis, goose fatty liver shows no obvious inflammation, fibrosis, and other pathological changes that are often seen in nonalcoholic fatty liver disease (**NAFLD**) of humans and mice. It can recover to normal state under certain conditions, indicating that goose has a unique protective mechanism (Hermier et al., 1999). Indeed, previous studies have identified some unique protective components, such as inhibition of complement system (Liu et al., 2016) and induction of mitochondria-related genes (Osman et al., 2016a), adiponectin receptor gene (Geng et al., 2016), and fatty acid desaturase genes (Osman et al., 2016b). Further uncovering the protective mechanism may

Received October 31, 2019.
Accepted August 10, 2020.

[1]Corresponding authors: tygeng@yzu.edu.cn (TG); yzgong@163.com (DG)

provide new ideas for developing methods to improve the quality and yield of goose fatty liver as well as to prevent and cure NAFLD in humans and other animals.

The development of NAFLD in humans and mice is not only related to intestinal microbes and metabolites but also closely related to the integrity of intestinal structure and the occurrence of inflammation (Schnabl and Brenner, 2014; Xin et al., 2014; Li et al., 2019). The "gut-liver axis" theory is often used to explain the interaction between the intestine and liver (Miura and Ohnishi, 2014). The intestine is the place where nutrients are digested and absorbed and also where intestinal microbes are colonized. When the number of harmful intestinal microbes are increased, their metabolites will lead to changes in intestinal structure and permeability (Wahlström, 2019). Direct contact between intestinal microbes and intestinal immune cells can induce inflammation (Mouzaki and Loomba, 2019). Increased permeability also increases the amount of microbes, their endotoxin (or lipopolysaccharide [**LPS**]), and harmful metabolites entering the intestine, causing systemic immune response, inflammation, and changes in the functions of other organs and tissues (Federico et al., 2017; Luci et al., 2019).

Data from previous molecular biology studies provide some insight into the relationship of gut microbes and their metabolites with intestinal structure and function. For example, supplementing *Clostridium butyricum* or its metabolite, butyric acid, to diet can induce the expression of tight junction-related genes, for example, occludin (***OCLN***) and tight junction protein ZO-1 (***TJP1***), in the intestine of mice (Li et al., 2018). The induction of these genes can improve intestinal structure and permeability, thus intestinal barrier is protected, direct contact between gut bacteria and immune cells is restricted, and the chance of LPS entering blood is reduced. On the contrary, if bad bacteria are increased and good bacteria are decreased in the intestine, the expression of tight junction-related genes may be downregulated, and the increased permeability of intestine allows gut bacteria get in touch with immune cells in the intestine, triggering immune response and inflammatory response (Lee, 2015). Pro/inflammatory cytokines such as tumor necrosis factor alpha (***TNFα***) and interleukin 1 beta (***IL1β***) can cause cell death and damage of intestinal structure and function (Schulzke et al., 2006; Al-Sadi et al., 2008). In the inflammatory response of intestine, sphingolipids, a group of bioactive lipids, may play an important role. It is known that the balance between ceramides and sphingosine-1-phosphate (**S1P**), the main species of sphingolipids, is key to cell survival, apoptosis, and inflammatory response in different physiological or pathological contexts (Nixon, 2009). There are a number of genes that can regulate the levels of ceramides and S1P, including serine palmitoyltransferase long-chain base subunit (***SPTLC***), dihydroceramide desaturase (***DEGS***), ceramide synthase (***CERS***), alkaline ceramidase (***ACER***), sphingosine-1-phosphate phosphatase (***SGPP***), N-acylsphingosine amidohydrolase (***ASAH***), and so on (Le Stunff et al., 2002; Coant et al., 2017). The balance between ceramides and S1P also determines the fate of a cell, and ceramides usually promote apoptosis while S1P usually promote cell growth (Guri et al., 2017; Gancheva et al., 2018). Apoptosis is a programmed cell death, which is different from necrosis (D'Arcy, 2019). Apoptosis is precisely controlled by a number of proteins including BCL2 apoptosis regulator (**BCL2**), BCL2 antagonist/killer 1 (**BAK1**), BH3 interacting domain death agonist (**BID**), phorbol-12-myristate-13-acetate–induced protein 1 (**PMAIP1**), caspases, and so on. Apoptosis is usually involved in remodeling of tissues and organs (e.g., intestinal atrophy) and does not induce pathological changes (e.g., inflammation) (Kawamoto et al., 2016). On the contrary, necrosis can cause inflammation and tissue injury (e.g., desquamation of intestine villi), and inflammation in turn promotes necrosis (Elmore, 2007; Grabinger et al., 2017). As sphingolipids can be synthesized with food-derived metabolites by intestinal cells or bacteria, intestinal hypertrophy or atrophy and functional strengthening or weakening may be closely associated with intestinal sphingolipid metabolism. In summary, intestinal structure and function are interconnected with gut bacteria and their metabolites and the expression of the genes related to sphingolipid metabolism, apoptosis, and cell growth, as well as inflammation and necrosis.

Compared with NAFLD in humans and mice, there are few studies on the relationship among the development of goose fatty liver, intestinal structure, and inflammation. In this study, we hypothesize that maintaining intestinal structural integrity to prevent occurrence of inflammation is a protective mechanism for goose fatty liver during the period of overfeeding. By addressing the hypothesis, this study may reveal the relationship between intestine and liver in the development of goose fatty liver, illustrate why inflammation does not occur in goose fatty liver, and open a new approach to improving the yield and quality of goose fatty liver and preventing the occurrence of nonalcoholic steatohepatitis suffered by other animals (e.g., tuning intestinal condition by supplementing probiotics to diet).

MATERIALS AND METHODS

Animals and Sample Collection

One hundred 1-day-old Landes geese were raised on floor in an open house in Licheng Livestock and Poultry Breeding Co., Ltd. (Huai'an, Jiangsu, China) with natural light, and the average temperature was from 10°C to 22°C. The geese were fed brooding diet (Supplementary Table 1) for the brooding period (1–28 d of age) and growing diet (Supplementary Table 2) for the growing period (29–65 d of age). The geese had free access to the diets and water. At the age of 66 d, 48 healthy geese were randomly divided into 2 groups, that is, the control group (which has free access to feed and water) and the overfeeding group, with 24 geese each group. The geese appeared to be active with tidy plumage and had normal feed intake and normal droppings, and their body

weights were around the average body weight. During the preoverfeeding (66–70 d of age) and overfeeding periods (71–94 d of age), the geese were raised in cages with one bird each cage in an open house at the company. The diet for the groups was the same in the periods, including the cooked corn plus 1% plant oil and 1% salt (Supplementary Table 3). For preoverfeeding, the feed intake for each goose was gradually increased from 100 to 300 g per day. For overfeeding, the following protocol was applied: the daily feed intake (3 meals a day) was 400 g for the first week, 600 g for the second week (4 meals a day), 800 g for the third week to the end (5 meals a day). This protocol was modified from that previously described one (Osman et al., 2016a).

On the 12th and 24th d of overfeeding, half of the geese from each group (12 geese each group) were randomly selected for sacrifice. The geese were fasted overnight before sample collection. The body weight of each goose was first measured, followed by blood collection. After cleaning with 75% alcohol, 2 mL of blood sample from each goose was subsequently collected from the right wing vein and then mixed with heparin sodium in collection tubes and placed on ice for 10 min. The plasma was transferred to a new Eppendorf Safe-Lock tube and stored at −20°C. The liver weight was measured. The intestine samples were only collected from the middle part of each intestinal segment (jejunum, ileum, and cecum), with one part (around 1-cm long) for histological analysis and another part for quantitative PCR (**qPCR**) analysis. For histological analysis, the intestine samples were fixed in 10% formalin overnight, followed by being stored in fresh 10% formalin. For qPCR analysis, the intestinal samples were rinsed with physiological saline 3 times, followed by being frozen in liquid nitrogen and stored in −70°C freezer.

All animal protocols were approved by the Animal Care and Use Committee of Yangzhou University.

Hematoxylin and Eosin Staining and Histomorphological Analysis

Hematoxylin and eosin staining was carried out according to the instructions of hematoxylin dye solution kit (Cat# G1005; Wuhan Servicebio Biotechnology Co., Ltd., Wuhan, China). After embedding with paraffin, sections were made, placed in water for section extension in seconds at 42°C, and dried for 2.5 h at 60°C. The sections were then placed in xylene for 20 min twice, ethanol for 5 min twice, 75% ethanol for 5 min, followed by washing with water more than 3 times. At the next step, the sections were dyed in hematoxylin for 3 to 5 min, after which the sections were placed in 1% hydrochloric acid solution for 3 to 5 s and 0.6 to 0.8% ammonia solution for 3 to 5 min. The sections were washed with water several times and dehydrated with 85 and 95% alcohol, followed by dyeing in eosin dye for 5 min. Subsequently, the sections were placed in ethanol for 5 min three times, in xylene for 5 min twice. Finally, the sections were sealed with neutral gum. The images of intestinal histological were acquired under a microscope (LY-WN-HP SUPER CCD; Chengdu Liyang precision machinery Co., Ltd., Chengdu, China) with a magnification of 100×, and the measurements on intestinal villus height and crypt depth were carried out at 5 positions (i.e., 5 bright fields with 2–3 villus each field under microscope) for each section.

Determination of Plasma LPS Concentration

The LPS concentration in plasma was determined according to the instructions for the LPS enzyme-linked immunosorbent assay (**ELISA**) kit (Cat# JL47951; Shanghai Jianglai Industrial Limited by Share Ltd., Shanghai, China). Briefly, blank, standard, and sample wells were set on a 96-well enzyme-labeled plate. In blank wells, no reagents and samples were added; in standard wells, 50 μL of different concentrations of standard LPS solutions were added; in sample wells, 40 μL of sample diluent and 10 μL of plasma were added. One hundred microliters of horseradish peroxidase solution (2 μg/mL) was then added to all wells except blank wells. The plate was incubated at 37°C for 60 min, followed by washing with detergent 5 times (adding detergent to wells and standing for 30 s each time). After detergent was completely discarded from the wells, 50 μL of the developer A and 50 μL of the developer B were added to the wells in turn, and the plate was incubated at 37°C for 15 min. Subsequently, the reaction was terminated by adding 50 μL of stop solution (At this time, the blue color turned into yellow.). The optical density (**OD**) values for standard and sample wells were sequentially read out after calibration with blank well at 450 nm. The concentrations and OD values of the standard solutions were then used to make the standard curve, and the linear regression equation for the standard curve was also calculated. Based on standard curve, the linear regression equation was used for calculation of actual plasma LPS concentration using OD value for each sample.

Total RNA Extraction, Reverse Transcription, and qPCR

Total RNA extraction, reverse transcription, and qPCR were carried out according to the methods previously described (Osman et al., 2016a). The primers were designed based on mRNA reference sequence published in GenBank (Table 1), with an exception for *TNFα* primers, which were designed using our local database established with RNA-seq data from transcriptome analysis of Landes goose. The primers have been described previously (Liu et al., 2016), and the specificity of the primers was verified by the melting cure in qPCR analysis. The forward primer is 5′-GTATGCAGCAACCCGTAG-3′, and the reverse primer is 5′-TGGCATTGCAATTTGGACA-3'. Glyceraldehyde-3-phosphate dehydrogenase (***GAPDH***) gene was used

Table 1. The sequences of primers for quantitative PCR

Gene	Accession number	Sequence (5′-3′)	Product size
GAPDH	XM_013199522	F-GCCATCAATGATCCCTTCAT R-CTGGGGTCACGCTCCTG	155
TJP1	XM_013177396.1	F-ACGCTGTTGAATGTCCC R-TCGAAGACTGCCGTTGC	216
OCLN	XM_013199669.1	F-GGAGCAGCCCAGCAAAG R-GCTTGAGGTCGGTGTCG	209
BID	XM_013172978.1	F-CCCCTCAGACCTGGAAC R-TGAAGACACGCTGTAGAA	101
PMAIP1	XM_013181610.1	F-CCAGCCCGAGTGAAGGAA R-GAACAGCTTTGCGATGAGGT	170
BCL2	XM_013187395.1	F-GATGACCGAGTACCTGAACC R-GCTCCCACCAGAACCAA	156
BAK1	XM_013197007.1	F-CAGCCCACCAAGGAGAA R-GAGGAAGCCCGTTATGC	153
IL1β	XM_013202125.1	F-CACAAGGACTTCGCCGACA R-CGCTCATCACGCAGGACA	163
SPTLC3	XM_013182212.1	F-CAGAAGACGACTGCACGAA R-CCCAACCACAACCACCC	145
ASAH2	XM_013178388.1	F-TTGTAAGTGCCAACCCT R-TGTGCCATTCAATCGTC	183
ACER1	XM_013200333.1	F-GTGGCTTTGCTGGCTCT R-AATGTTGGCATCTCGTAG	135
CERS6	XM_013171147.1	F-TTTCCTGCCTTGTGGGT R-TTCGGTCATCCTTTGCTAC	130
SGPP2	XM_013181451.1	F-ACTATTACAGCCCTACCCG R-AACCTCCAGCCTCCTCC	293
DEGS2	XM_013177434.1	F-ATCCCTTACTCTGCCTCCTT R-GGTTCACATACAACGGTCTCA	184

as internal reference gene. The data from qPCR were analyzed with $2^{-\Delta\Delta Ct}$ method using Ct value.

Statistical Analysis

All the data were expressed as the means ± SEM. Student *t* test was used to analyze statistical significance of the difference between the treatment and the control groups, and $P < 0.05$ was set as the criteria of statistical significance.

RESULTS

Fatty Liver Was Successfully Induced by Overfeeding

Consistent with previous reports, the body weight, weight gain, liver weight, and the ratio of liver weight to body weight in the overfed geese were significantly higher than those in the control geese (Table 2), and the liver color in the overfed geese appeared to be light yellow while the liver color in the control geese appeared to be red, which indicated that fatty liver was successfully induced by overfeeding in the overfed geese.

Effect of Overfeeding on Intestinal Histological Structure

The hematoxylin and eosin staining analysis of different intestinal segments (jejunum, ileum, and cecum) in the overfeeding and control groups on the 12th and 24th d of overfeeding showed that the intestines of the overfed and the control geese exhibited intact histological structure and orderly arrangement. Except for the atrophy of cecum in the overfed geese at the late stage of overfeeding, the intestinal villi of the 2 groups grew well, and there were no obvious tissue damage and pathological changes (Figure 1). This similarity in intestinal structure between the overfed and control geese indicated that overfeeding did not damage the integrity of goose intestinal structure and cause pathological symptoms such as inflammation and injury.

Moreover, on the 12th d of overfeeding, compared with the control group, the villus height of ileum, the crypt depth of jejunum, and the villus-to-crypt ratio of ileum in the overfeeding group were significantly increased, but the villus-to-crypt ratio of jejunum was significantly decreased (Table 3). On the 24th d of overfeeding, compared with the control group, the villus heights of

Table 2. Average body weight, liver weight, and the ratio of liver to body weights in the overfed and control geese during the period of overfeeding

Day	Variable (g)	Control	Overfeeding	*P* value
0	Body weight	372.18 ± 18.98	371.64 ± 20.47	>0.05
12	Body weight	4202.86 ± 255.52	5,023 ± 231.27	<0.01
	Weight gain	482 ± 354.75	1,300 ± 283.07	<0.01
	Liver weight	116.63 ± 22.57	352.19 ± 60.51	<0.01
	Liver/Body (%)	2.76 ± 0.44	7.01 ± 1.08	<0.01
24	Body weight	4,415 ± 382.95	6867.20 ± 446.65	<0.01
	Weight gain	692 ± 459.54	3,226 ± 504.8	<0.01
	Liver weight	102.95 ± 23.46	830.19 ± 157.08	<0.01
	Liver/Body (%)	2.33 ± 0.47	12.09 ± 2.12	<0.01

The body weight, weight gain, and liver weight of the control and overfed geese (overfeeding) were determined on the 12th and 24th d of overfeeding. The ratio of liver weight to body weight was also calculated. n = 12. The values are presented as the means ± SEM.

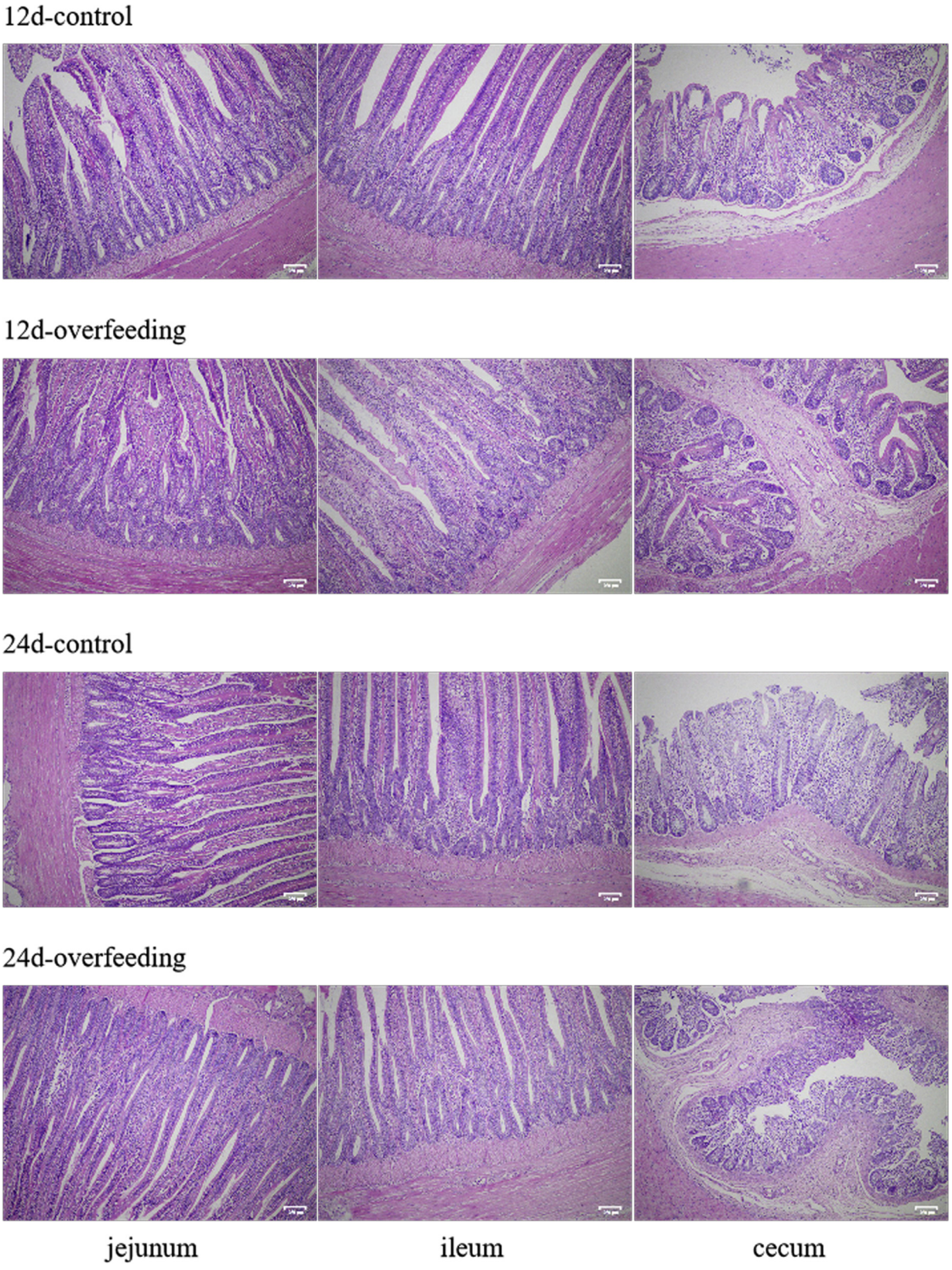

Figure 1. The effect of overfeeding on villus height and crypt depth of jejunum, ileum, and cecum in the overfed vs. control (normally fed) Landes geese. The sections of intestine were hematoxylin and eosin stained. The images were acquired under a microscope with magnification 100×; the size unit of the photograph was 150 μm. The intestinal morphology of jejunum, ileum, and cecum collected on the 12th and 24th d of overfeeding.

jejunum and ileum and the villus-to-crypt ratio of ileum were significantly increased in the overfed geese, but the villus height of cecum was significantly decreased (Table 3). Therefore, the data indicated that overfeeding promoted cell proliferation and the capacities of digestion and absorption of ileum during the period of overfeeding, and that of jejunum at the late stage of overfeeding, but inhibited that of the jejunum at the

early stage of overfeeding and that of the cecum at the late stage of overfeeding.

Effects of Overfeeding on the Expression of Intestinal Tight Junction-Related Genes and Plasma LPS Concentration

OCLN and *TJP1* genes are closely related to intestinal structural integrity and permeability. In this study, the expression of *OCLN* and *TJP1* in different intestinal segments of the overfed and control geese was determined by qPCR during the period of overfeeding. The results showed that there was no significant difference in the expression of *TJP1* and *OCLN* genes in jejunum, ileum, and cecum between the overfed and control geese (Figures 2A, 2B), except that the expression of *TJP1* in ileum was significantly decreased in the overfed vs. control geese at the late stage of overfeeding. These findings further confirmed that the overall effect of overfeeding on structural integrity and permeability of goose intestine was negligible. More importantly, the plasma LPS concentrations of the control and overfed geese were quite similar to each other during the period of overfeeding (Figure 2C).

Effects of Overfeeding on the Expression of Inflammation and Apoptosis-Related Genes in Goose Intestine

Intestinal integrity and permeability are affected by inflammation. In this study, the expression of *TNFα* and *IL1β* in the intestine of the overfed and control geese was determined by qPCR at the late stage of overfeeding. The results showed that there was no significant difference in the expression of *TNFα* and *IL1β* between the groups (Figures 3A, 3B).

As mentioned previously, the cecum of the overfed geese exhibited atrophy at the later stage of overfeeding, and the inflammation was not the cause of the atrophy, we speculated that apoptosis could be involved in the atrophy of the cecum in the overfed geese. To verify this, the expression of apoptosis-related genes, including *BID*, *PMAIP1*, *BCL2*, and *BAK1*, was determined in the cecum of the overfed and control geese at the late stage of overfeeding by qPCR. The data showed that, compared with the control group, the expression of *PMAIP1* ($P = 0.108$) and *BCL2* ($P < 0.05$) in the cecum of the overfed geese was increased (Figure 3C).

Effects of Overfeeding on the Expression of Sphingolipid Metabolism-Related Genes in Goose Intestine

To understand the effect of overfeeding on the increase of ileal villus height and the atrophy of cecum in the overfeeding group, the expression of some representative genes related to sphingolipid metabolism was determined. Compared with the control group, the expression of *SPTLC3* (2.1-folds of upregulations, $P < 0.01$) and *ASAH2* (19.9-folds of upregulation, $P = 0.083$) was increased and that of *ACER1* (9.8-folds of downregulation, $P = 0.076$) and *DEGS2* (1.5-folds of downregulation, $P < 0.05$) was decreased in the ileum of the overfed geese (Figure 4A); the expression of *SPTLC3* (1.5-folds of upregulation, $P = 0.055$) and *CERS6* (12.2-folds of upregulation, $P = 0.052$) was increased and that of *ACER1* (3.1-folds of downregulation, $P < 0.05$), *SGPP2* (3.4-folds of downregulation, $P < 0.01$), and *DEGS2* (2.6-folds of downregulation, $P < 0.01$) was decreased in the cecum of the overfed goose (Figure 4B).

Table 3. The villus height, crypt depth and the ratio of villus height to crypt depth in the jejunum, ileum and cecum of the control and overfed geese during the period of overfeeding (μm)

Day	Tissue	Variable	Control	Overfeeding	*P* value
12	Jejunum	Villus height	1122.58 ± 255.31	1057.75 ± 219.28	>0.05
		Crypt depth	307.78 ± 66.34	382.25 ± 13.94	<0.05
		Villus/Crypt	3.65 ± 0.43	2.75 ± 0.46	<0.05
	Ileum	Villus height	831.29 ± 65.67	1189.86 ± 181.54	<0.01
		Crypt depth	260.85 ± 38.09	274.09 ± 83.38	>0.05
		Villus/Crypt	3.22 ± 0.27	4.52 ± 0.82	<0.05
	Cecum	Villus height	240.21 ± 19.45	222.03 ± 44.67	>0.05
		Crypt depth	133.70 ± 21.95	118.72 ± 13.78	>0.05
		Villus/Crypt	1.82 ± 0.16	1.86 ± 0.19	>0.05
24	Jejunum	Villus height	1101.81 ± 140.97	1437.45 ± 127.63	<0.01
		Crypt depth	314.67 ± 23.06	336.64 ± 77.78	>0.05
		Villus/Crypt	3.49 ± 0.22	3.86 ± 0.97	>0.05
	Ileum	Villus height	1040.77 ± 31.40	1342.46 ± 154.48	<0.01
		Crypt depth	288.05 ± 60.61	299.57 ± 36.90	>0.05
		Villus/Crypt	3.72 ± 0.62	4.49 ± 0.29	<0.05
	Cecum	Villus height	255.57 ± 21.36	144.25 ± 40.08	<0.01
		Crypt depth	164.41 ± 19.73	140.04 ± 34.39	>0.05
		Villus/Crypt	1.42 ± 0.23	1.28 ± 0.37	>0.05

The villus height and crypt depth of the control and overfed geese were measured on the 12th and 24th d of overfeeding (Measurements were carried out at 5 locations each section.). The ratio of villus height to crypt depth was also calculated. n = 5. The values are presented as the means ± SEM.

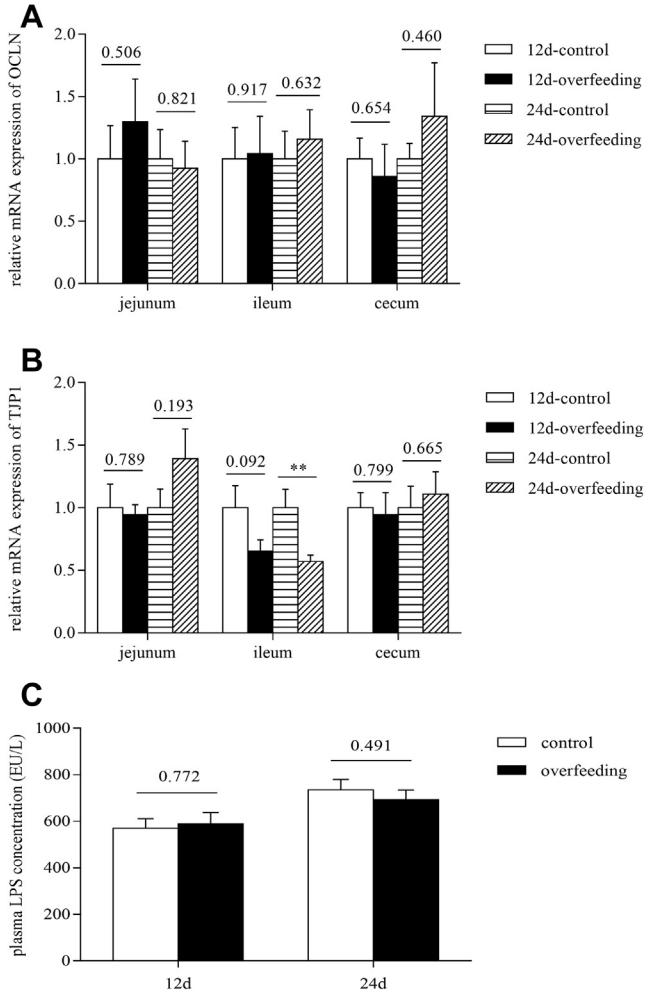

Figure 2. Effects of overfeeding on the expression of intestinal tight junction-related genes and plasma lipopolysaccharide (LPS) concentration. The gene expression was determined by quantitative PCR. The expression of *OCLN* and *TJP1* genes in jejunum, ileum, and cecum of the overfed vs. control (normally-fed) geese was determined on the 12^{th} d (A) and 24^{th} d (B) of overfeeding. The gene expression of the overfed geese was presented as the fold change over the control at each time point. n = 6. (C) The plasma LPS concentration in the overfed vs. control geese was determined by the ELISA kit. n = 12. The values shown on the top of the columns denote *P* values; ** denotes $P < 0.01$ vs. control. All the data are presented as the means ± SEM.

DISCUSSION

Intestinal microbes and metabolites are involved in the development of NAFLD in humans and mice (Soderborg and Friedman, 2018; Chu et al., 2019). Harmful intestinal microbes and metabolites can cause changes in the structural integrity and permeability of intestine, damage the intestinal protective barrier, and induce intestinal and systemic immune response, thus leading to liver inflammation and injury through the gut-liver axis (Ong and Yim, 2017). In this study, data showed that the structural integrity of each intestinal segment was not damaged during the development of goose fatty liver. On one hand, the villi of each intestinal segment were arranged orderly, the crypt were distinct, and the histological structure was intact without special pathological symptoms in both the overfed and control geese. On the other hand, there was generally no significant difference in the expression of tight junction marker genes (*OCLN*, *TJP1*) and plasma LPS concentration between the 2 groups. In addition, the expression of inflammation marker genes (*TNFα* and *IL1β*) in the intestine of the overfed geese was similar to that in the control geese, indicating that intestinal inflammation did not occur during the overfeeding period, which further supported the viewpoint that intestinal histological structure remained intact during the overfeeding period. Intestinal histological integrity and no inflammation are conducive to maintaining the digestive and absorptive capacity of intestine for nutrients, promoting the formation of goose fatty liver, avoiding the harmful effects caused by invasion of intestinal microbes and metabolites, and maintaining the normal function of the liver (Artis, 2008; Cerf-Bensussan and Gaboriau-Routhiau, 2010; Kirpich et al., 2015). This is essential for the super tolerance of goose liver to severe steatosis. As for the reason why intestinal inflammation does not occur in goose, it may be related to short-chain fatty acids produced by beneficial bacteria, as demonstrated by previous studies (Seo et al., 2013; Liu et al., 2016).

This study also found that the ileal villus height was increased, the crypt became shallow, and the ratio of villus to crypt was increased in the overfed vs. control geese, while that of the cecum was changed inversely at the late stage of overfeeding. As intestinal villus height, crypt depth, and the villus-to-crypt ratio can reflect the proliferative capacity and the digestive and absorptive capacities of intestinal epithelial cells (Magnotti and Deitch, 2005; Lamb-Rosteski et al., 2008), the ileal histological changes in the overfed geese indicated that the proliferation of epithelial cells was promoted and the digestive and absorptive capacities were enhanced. Ileum may be the main contributor to the enhanced capacity of nutrient digestion and absorption. Similarly, the opposite histological changes of the cecum indicated that the adaptation of the cecum to overfeeding weakened its function. The change in the expression of the genes involved in sphingolipid synthesis and metabolism (*SPTLC*, *DEGS*, *CERS*, *ACER*, *SGPP*, *ASAH*) may provide a clue to ileal hypertrophy and cecal atrophy as sphingolipids do not only participate in the construction of cell membranes (Hawthorne, 1975; Coant et al., 2017) but also participate in cell growth and apoptosis and signal transduction of complex biological functions such as inflammation and immunity (Coant et al., 2017; Ogretmen, 2018). The major active sphingolipids are ceramides and S1P which usually have opposite effects. Ceramides can promote cell apoptosis (Hannun and Obeid, 2008), while S1P can promote cell survival and differentiation (Hait et al., 2006; Hannun and Obeid, 2008), so the balance between ceramides and S1P determines the fate of cells (Guri et al., 2017; Gancheva et al., 2018). In addition, ceramides and S1P also affect the expression of inflammatory genes (Fang et al., 2019). The balance between ceramide and S1P is determined by a number of genes involved in the metabolism of ceramide and S1P.

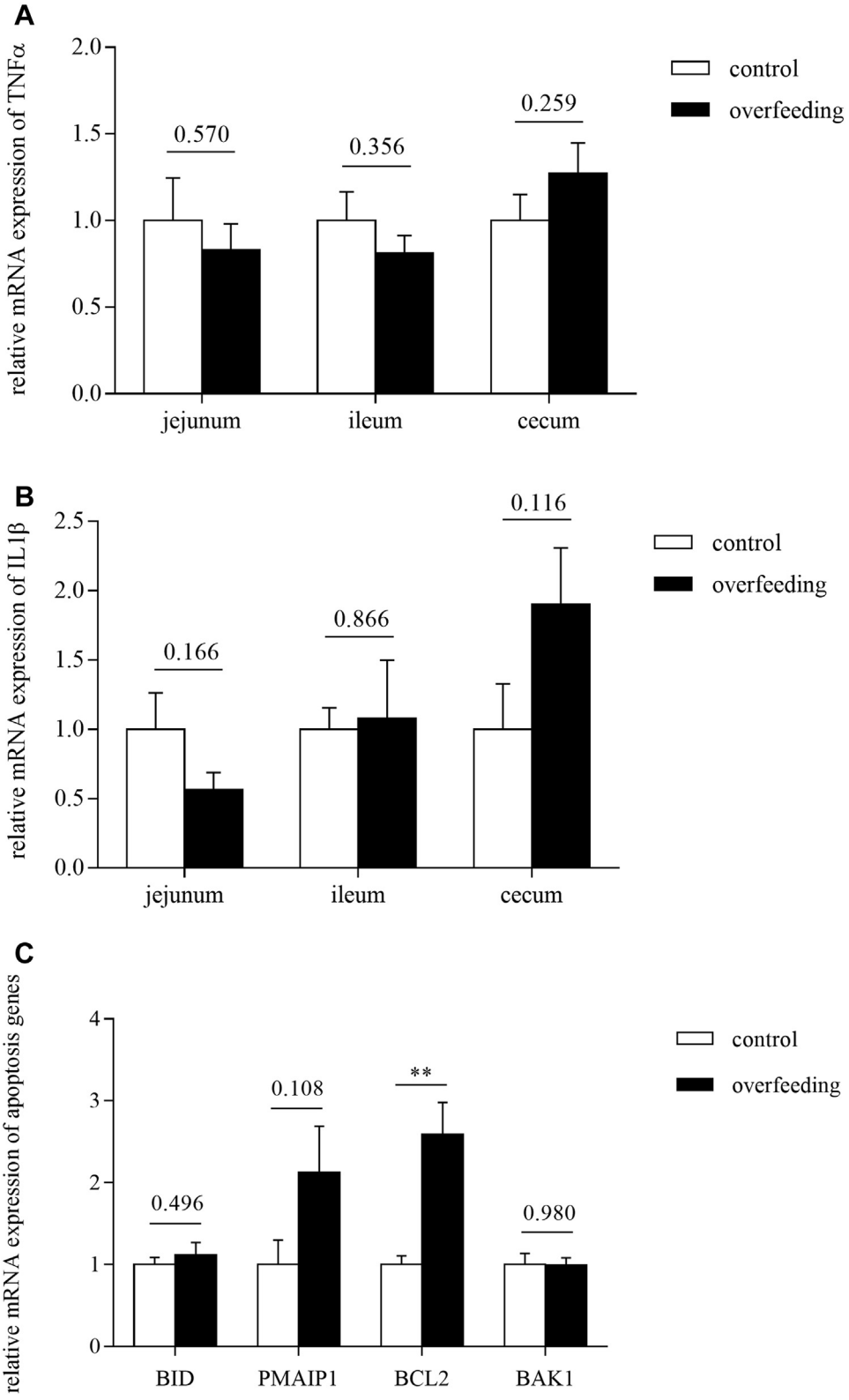

Figure 3. Effects of overfeeding on the expression of inflammation and apoptosis-related genes in goose intestine. The gene expression was determined by quantitative PCR. (A, B) The expression of *TNFα* and *IL1β* genes in jejunum, ileum, and cecum of the overfed vs. control (normally fed) geese was determined on the 24th d of overfeeding. (C) The expression of *BID*, *PMAIP1*, *BCL2*, and *BAK1* genes in cecum of the overfed vs. control (normally fed) geese was determined on the 24th d of overfeeding. The gene expression of the overfed geese was presented as the fold change over the control. n = 6. The values shown on the top of the columns denote P values; ** denotes $P < 0.01$ vs. control. All the data are presented as the means ± SEM.

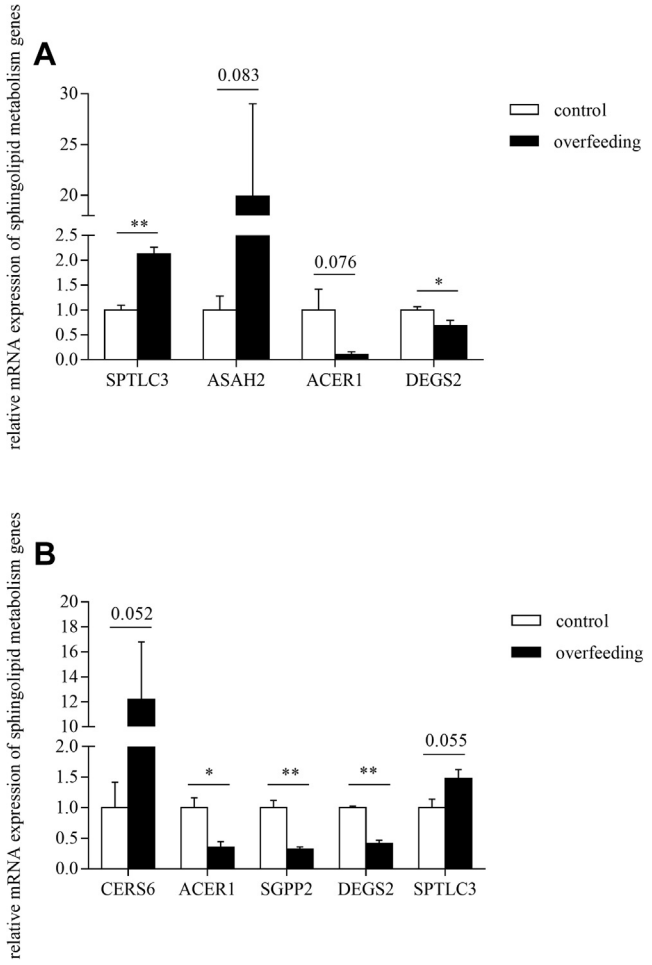

Figure 4. Effects of overfeeding on the expression of sphingolipid metabolism–related genes in goose intestine. The gene expression was determined by quantitative PCR. (A) The expression of *SPTLC3*, *ASAH2*, *ACER1*, and *DEGS2* genes in ileum of the overfed vs. control (normally fed) geese was determined on the 24th d of overfeeding. (B) The expression of *CERS6*, *ACER1*, *SGPP2*, *DEGS2*, and *SPTLC3* genes in cecum of the overfed vs. control (normally fed) geese was determined on the 24th d of overfeeding. The gene expression of the overfed geese was presented as the fold change over the control. n = 4. The values shown on the top of the columns denote *P* values; *, ** denotes $P < 0.05$ or 0.01 vs. control. All the data are presented as the means ± SEM.

Ceramide can be generated through 3 different pathways, that is, the *de novo* pathway, the sphingomyelinase pathway, and the salvage pathway (Le Stunff et al., 2002). SPTLC has 3 isoforms, SPTLC1-3, which are the first and rate-limiting enzymes in the *de novo* pathway, promoting the synthesis of 3-ketosphinganine (Chaurasia et al., 2016). The latter is then converted into sphinganine by 3-ketosphinganine reductase. Subsequently, ceramide synthases convert sphinganine to dihydroceramide (Schiffmann et al., 2009), with which ceramide is synthesized by DEGS (Jang et al., 2017). Previous studies have shown that inhibition of SPTLC activity can reduce ceramide levels in cell lines or rodents (Ruangsiriluk et al., 2012), and CERS6 has a proapoptotic effect as it can serve an essential downstream mediator of p53-dependent apoptosis by interacting with p53-upregulated modulator of apoptosis (Fekry et al., 2016). On the other hand, ceramidases promote ceramide degradation and sphingosine synthesis (Govindarajah et al., 2019). For example, ACER1 can catalyze the hydrolysis of very-long-chain ceramides to generate sphingosine (Sun et al., 2008), while ASAH2 can catalyze hydrolysis of the N-acyl linkage of ceramide to produce sphingosine. Enzymatic inhibition or knockout of ASAH2 reduces sphingosine levels (Kono et al., 2006), increases ceramide levels, and promotes apoptosis (García-Barros et al., 2016), which is consistent with a previous finding that ASAH2 has a role in maintaining intestinal barrier in a mouse model of inflammatory bowel disease (Snider et al., 2012). In addition, SGPPs promote the salvage and recycling of sphingosine into long-chain ceramides (Terragni et al., 2014) by catalyzing the degradation of S1P (Schwiebs et al., 2017). In mice, knockout of SGPP2 can inhibit dextran sodium sulfate–induced intestinal epithelial cell apoptosis and systemic inflammatory response and improve mucosal barrier integrity (Huang et al., 2016). The data in this study showed that the synthesis of sphingolipids (*SPTLC3*) and the degradation of ceramide (*ASAH2*) were increased in the ileum of the overfed vs. control geese. Increased synthesis of sphingolipids and degradation of ceramides in the ileum may promote the proliferation of intestinal epithelial cells and increase of villus height. On the contrary, the synthesis of ceramides was increased (*CERS6*) and the ceramide degradation was decreased (*ACER1*) in the cecum during the overfeeding period. Increased ceramide synthesis and decreased ceramide degradation in cecum may promote apoptosis of intestinal epithelial cell, decrease villus height, and cause atrophy. Apoptosis as a programmed cell death can facilitate the removal of the damaged and dysfunctional cells by breaking the cells into membrane-bound, ultrastructurally well-preserved fragments, followed by ingestion of macrophages (Kaczanowski, 2016). Therefore, apoptosis can preserve the integrity and structure of surrounding tissue without induction of inflammation (Sankari et al., 2012; Kaczanowski, 2016). In line with this, the expression of apoptotic genes (*BCL2*, *PMAIP1*) was increased in the cecum of the overfed vs. control geese at the late stage of overfeeding, suggesting that apoptotic signaling pathway in the cecum of the overfed geese might be activated at the late stage of overfeeding (Britt et al., 2019). However, triggering apoptosis requires a cascade of reactions with a number of proteins including BCL2, BID, BAK, BAX, caspases (Mullen and Obeid, 2012), and so on; thus, the change in the mRNA expression of *BCL2* and *PMAIP1* just hints the occurrence of apoptosis, which needs a validation with determination of activation of these proteins. In one word, the consistency of the expression of sphingolipid metabolism–related genes with the histological changes of ileum and cecum of goose induced by overfeeding indicates that sphingolipid metabolism may play an important role in goose intestinal adaptation to overfeeding.

In conclusion, maintenance of intestinal structure integrity, sphingolipid-mediated ileal hypertrophy, and

apoptosis-mediated cecal atrophy is essential for goose fatty liver to prevent inflammation and development.

ACKNOWLEDGMENTS

This work was supported by the National Natural Science Foundation of China (31672405, 31972546), Joint International Research Laboratory of Agriculture and Agri-Product Safety of the Ministry of Education of China, and the Priority Academic Program Development of Jiangsu Higher Education Institutions.

Conflicts of Interest Statement: The authors claim no conflict of interest.

SUPPLEMENTARY DATA

Supplementary data associated with this article can be found in the online version at https://doi.org/10.1016/j.psj.2020.08.052.

REFERENCES

Al-Sadi, R., D. Ye, K. Dokladny, and T. Y. Ma. 2008. Mechanism of IL-1beta-induced increase in intestinal epithelial tight junction permeability. J. Immunol. 180:5653–5661.

Artis, D. 2008. Epithelial-cell recognition of commensal bacteria and maintenance of immune homeostasis in the gut. Nat. Rev. Immunol. 8:411–420.

Britt, E. L., S. Raman, K. Leek, C. H. Sheehy, S. W. Kim, and H. Harada. 2019. Combination of fenretinide and ABT-263 induces apoptosis through NOXA for head and neck squamous cell carcinoma treatment. PLoS One 14:e0219398.

Cerf-Bensussan, N., and V. Gaboriau-Routhiau. 2010. The immune system and the gut microbiota: friends or foes? Nat. Rev. Immunol. 10:735–744.

Chaurasia, B., V. A. Kaddai, G. I. Lancaster, D. C. Henstridge, S. Sriram, D. L. Galam, V. Gopalan, K. N. Prakash, S. S. Velan, S. Bulchand, T. J. Tsong, M. Wang, M. M. Siddique, G. Yuguang, K. Sigmundsson, N. A. Mellet, J. M. Weir, P. J. Meikle, M. S. Bin M. Yassin, A. Shabbir, J. A. Shayman, Y. Hirabayashi, S. T. Shiow, S. Sugii, and S. A. Summers. 2016. Adipocyte ceramides regulate subcutaneous adipose browning, inflammation, and metabolism. Cell Metab. 24:820–834.

Chu, H., Y. Duan, L. Yang, and B. Schnabl. 2019. Small metabolites, possible big changes: a microbiota-centered view of non-alcoholic fatty liver disease. Gut 68:359–370.

Coant, N., W. Sakamoto, C. Mao, and Y. A. Hannun. 2017. Ceramidases, roles in sphingolipid metabolism and in health and disease. Adv. Biol. Regul. 63:122–131.

D'Arcy, M. S. 2019. Cell death: a review of the major forms of apoptosis, necrosis and autophagy. Cell Biol. Int. 43:582–592.

Elmore, S. 2007. Apoptosis: a review of programmed cell death. Toxicol. Pathol. 35:495–516.

Fang, Z., S. Pyne, and N. J. Pyne. 2019. Ceramide and sphingosine 1-phosphate in adipose dysfunction. Prog. Lipid Res. 74:145–159.

Federico, A., M. Dallio, G. G. Caprio, V. M. Ormando, and C. Loguercio. 2017. Gut microbiota and the liver. Minerva Gastroenterol. Dietol. 63:385–398.

Fekry, B., K. A. Jeffries, A. Esmaeilniakooshkghazi, B. Ogretmen, S. A. Krupenko, and N. I. Krupenko. 2016. CerS6 is a novel transcriptional target of p53 protein activated by non-genotoxic stress. J. Biol. Chem. 291:16586–16596.

Gancheva, S., T. Jelenik, E. Álvarez-Hernández, and M. Roden. 2018. Interorgan metabolic crosstalk in human insulin resistance. Physiol. Rev. 98:1371–1415.

García-Barros, M., N. Coant, T. Kawamori, M. Wada, A. J. Snider, J. P. Truman, B. X. Wu, H. Furuya, C. J. Clarke, A. B. Bialkowska, A. Ghaleb, V. W. Yang, L. M. Obeid, and Y. A. Hannun. 2016. Role of neutral ceramidase in colon cancer. FASEB J. 30:4159–4171.

Geng, T., B. Yang, F. Li, L. Xia, Q. Wang, X. Zhao, and D. Gong. 2016. Identification of protective components that prevent the exacerbation of goose fatty liver: characterization, expression and regulation of adiponectin receptors. Comp. Biochem. Physiol. B Biochem. Mol. Biol. 194-195:32–38.

Govindarajah, N., R. Clifford, D. Bowden, P. A. Sutton, J. L. Parsons, and D. Vimalachandran. 2019. Sphingolipids and acid ceramidase as therapeutic targets in cancer therapy. Crit. Rev. Oncol. Hematol. 138:104–111.

Grabinger, T., K. J. Bode, J. Demgenski, C. Seitz, M. E. Delgado, F. Kostadinova, C. Reinhold, N. Etemadi, S. Wilhelm, M. Schweinlin, K. Hänggi, J. Knop, C. Hauck, H. Walles, J. Silke, H. Wajant, U. Nachbur, W. Wei-Lynn W, and T. Brunner. 2017. Inhibitor of apoptosis protein-1 regulates tumor necrosis factor-mediated destruction of intestinal epithelial cells. Gastroenterology 152:867–879.

Guri, Y., M. Colombi, E. Dazert, S. K. Hindupur, J. Roszik, S. Moes, P. Jenoe, M. H. Heim, I. Riezman, H. Riezman, and M. N. Hall. 2017. mTORC2 promotes tumorigenesis via lipid synthesis. Cancer Cell 32:807–823.e12.

Hait, N. C., C. A. Oskeritzian, S. W. Paugh, S. Milstien, and S. Spiegel. 2006. Sphingosine kinases, sphingosine 1-phosphate, apoptosis and diseases. Biochim. Biophys. Acta 1758:2016–2026.

Hannun, Y. A., and L. M. Obeid. 2008. Principles of bioactive lipid signalling: lessons from sphingolipids. Nat. Rev. Mol. Cell Biol. 9:139–150.

Hawthorne, J. N. 1975. A note on the life of J.L.W. Thudichum (1829-1901). Biochem. Soc. Trans. 3:591.

Hermier, D. 1997. Lipoprotein metabolism and fattening in poultry. J. Nutr. 127:805S–808S.

Hermier, D., D. Rousselot-Pailley, R. Peresson, and N. Sellier. 1994. Influence of orotic acid and estrogen on hepatic lipid storage and secretion in the goose susceptible to liver steatosis. Biochim. Biophys. Acta 1211:97–106.

Hermier, D., M. R. Salichon, G. Guy, and R. Peresson. 1999. Differential channelling of liver lipids in relation to susceptibility to hepatic steatosis in the goose. Poult. Sci. 78:1398–1406.

Huang, W. C., J. Liang, M. Nagahashi, D. Avni, A. Yamada, M. Maceyka, A. R. Wolen, T. Kordula, S. Milstien, K. Takabe, T. Oravecz, and S. Spiegel. 2016. Sphingosine-1-phosphate phosphatase 2 promotes disruption of mucosal integrity, and contributes to ulcerative colitis in mice and humans. FASEB J. 30:2945–2958.

Jang, Y., X. Rao, and Q. Jiang. 2017. Gamma-tocotrienol profoundly alters sphingolipids in cancer cells by inhibition of dihydroceramide desaturase and possibly activation of sphingolipid hydrolysis during prolonged treatment. J. Nutr. Biochem. 46:49–56.

Kaczanowski, S. 2016. Apoptosis: its origin, history, maintenance and the medical implications for cancer and aging. Phys. Biol. 13:031001.

Kawamoto, Y., Y. I. Nakajima, and E. Kuranaga. 2016. Apoptosis in cellular society: communication between apoptotic cells and their neighbors. Int. J. Mol. Sci. 17:2144.

Kirpich, I. A., L. S. Marsano, and C. J. McClain. 2015. Gut-liver axis, nutrition, and non-alcoholic fatty liver disease. Clin. Biochem. 48:923–930.

Kono, M., J. L. Dreier, J. M. Ellis, M. L. Allende, D. N. Kalkofen, K. M. Sanders, J. Bielawski, A. Bielawska, Y. A. Hannun, and R. L. Proia. 2006. Neutral ceramidase encoded by the Asah2 gene is essential for the intestinal degradation of sphingolipids. J. Biol. Chem. 281:7324–7331.

Lamb-Rosteski, J. M., L. D. Kalischuk, G. D. Inglis, and A. G. Buret. 2008. Epidermal growth factor inhibits Campylobacter jejuni-induced claudin-4 disruption, loss of epithelial barrier function, and Escherichia coli translocation. Infect. Immun. 76:3390–3398.

Le Stunff, H., C. Peterson, H. Liu, S. Milstien, and S. Spiegel. 2002. Sphingosine-1-phosphate and lipid phosphohydrolases. Biochim. Biophys. Acta 1582:8–17.

Lee, S. H. 2015. Intestinal permeability regulation by tight junction: implication on inflammatory bowel diseases. Intest. Res. 13:11–18.

Li, H., Y. Gong, Y. Xie, Q. Sun, and Y. Li. 2018. Clostridium butyricum protects the epithelial barrier by maintaining tight junction protein expression and regulating microflora in a murine model of

dextran sodium sulfate-induced colitis. Scand. J. Gastroenterol. 53:1031–1042.
Li, W., H. Yang, Q. Zhao, X. Wang, J. Zhang, and X. Zhao. 2019. Polyphenol-rich loquat fruit extract prevents fructose-induced nonalcoholic fatty liver disease by modulating glycometabolism, lipometabolism, oxidative stress, inflammation, intestinal barrier, and gut microbiota in mice. J. Agric. Food Chem. 67:7726–7737.
Liu, L., X. Zhao, Q. Wang, X. Sun, L. Xia, Q. Wang, B. Yang, Y. Zhang, S. Montgomery, H. Meng, T. Geng, and D. Gong. 2016. Prosteatotic and protective components in a unique model of fatty liver: gut microbiota and suppressed complement system. Sci. Rep. 6:31763.
Luci, C., E. Vieira, T. Perchet, P. Gual, and R. Golub. 2019. Natural killer cells and type 1 innate lymphoid cells are new actors in nonalcoholic fatty liver disease. Front. Immunol. 10:1192.
Magnotti, L. J., and E. A. Deitch. 2005. Burns, bacterial translocation, gut barrier function, and failure. J. Burn Care Rehabil. 26:383–391.
Miura, K., and H. Ohnishi. 2014. Role of gut microbiota and Toll-like receptors in nonalcoholic fatty liver disease. World J. Gastroenterol. 20:7381–7391.
Mouzaki, M., and R. Loomba. 2019. Insights into the evolving role of the gut microbiome in nonalcoholic fatty liver disease: rationale and prospects for therapeutic intervention. Pages 1-17 in Therap. Adv. Gastroenterol. 12.
Mullen, T. D., and L. M. Obeid. 2012. Ceramide and apoptosis: exploring the enigmatic connections between sphingolipid metabolism and programmed cell death. Anticancer Agents Med. Chem. 12:340–363.
Nixon, G. F. 2009. Sphingolipids in inflammation: pathological implications and potential therapeutic targets. Br. J. Pharmacol. 158:982–993.
Ogretmen, B. 2018. Sphingolipid metabolism in cancer signalling and therapy. Nat. Rev. Cancer 18:33–50.
Ong, H. S., and H. C. H. Yim. 2017. Microbial factors in inflammatory diseases and cancers. Adv. Exp. Med. Biol. 1024:153–174.
Osman, R. H., D. Shao, L. Liu, L. Xia, X. Sun, Y. Zheng, L. Wang, R. Zhang, Y. Zhang, J. Zhang, D. Gong, and T. Geng. 2016a. Expression of mitochondria-related genes is elevated in overfeeding-induced goose fatty liver. Comp. Biochem. Physiol. B Biochem. Mol. Biol. 192:30–37.
Osman, R. H., L. Liu, L. Xia, X. Zhao, Q. Wang, X. Sun, Y. Zhang, B. Yang, Y. Zheng, D. Gong, and T. Geng. 2016b. Fads1 and 2 are promoted to meet instant need for long-chain polyunsaturated fatty acids in goose fatty liver. Mol. Cell. Biochem. 418:103–117.
Ruangsiriluk, W., S. E. Grosskurth, D. Ziemek, M. Kuhn, S. G. des Etages, and O. L. Francone. 2012. Silencing of enzymes involved in ceramide biosynthesis causes distinct global alterations of lipid homeostasis and gene expression. J. Lipid Res. 53:1459–1471.
Sankari, S. L., K. M. Masthan, N. A. Babu, T. Bhattacharjee, and M. Elumalai. 2012. Apoptosis in cancer–an update. Asian Pac. J. Cancer Prev. 13:4873–4878.
Sanyal, A. J., E. M. Brunt, D. E. Kleiner, K. V. Kowdley, N. Chalasani, J. E. Lavine, V. Ratziu, and A. McCullough. 2011. Endpoints and clinical trial design for nonalcoholic steatohepatitis. Hepatology 54:344–353.
Schiffmann, S., J. Sandner, R. Schmidt, K. Birod, I. Wobst, H. Schmidt, C. Angioni, G. Geisslinger, and S. Grösch. 2009. The selective COX-2 inhibitor celecoxib modulates sphingolipid synthesis. J. Lipid Res. 50:32–40.
Schnabl, B., and D. A. Brenner. 2014. Interactions between the intestinal microbiome and liver diseases. Gastroenterology 146:1513–1524.
Schulzke, J. D., C. Bojarski, S. Zeissig, F. Heller, A. H. Gitter, and M. Fromm. 2006. Disrupted barrier function through epithelial cell apoptosis. Ann. N. Y. Acad. Sci. 1072:288–299.
Schwiebs, A., D. Thomas, B. Kleuser, J. M. Pfeilschifter, and H. H. Radeke. 2017. Nuclear translocation of sgpp-1 and decrease of sgpl-1 activity contribute to sphingolipid rheostat regulation of inflammatory dendritic cells. Mediators Inflamm. 2017:5187368.
Seo, M., I. Inoue, M. Tanaka, N. Matsuda, T. Nakano, T. Awata, S. Katayama, D. H. Alpers, and T. Komoda. 2013. Clostridium butyricum MIYAIRI 588 improves high-fat diet-induced non-alcoholic fatty liver disease in rats. Dig. Dis. Sci. 58:3534–3544.
Snider, A. J., B. X. Wu, R. W. Jenkins, J. A. Sticca, T. Kawamori, Y. A. Hannun, and L. M. Obeid. 2012. Loss of neutral ceramidase increases inflammation in a mouse model of inflammatory bowel disease. Prostaglandins Other Lipid Mediat. 99:124–130.
Soderborg, T. K., and J. E. Friedman. 2018. Imbalance in gut microbes from babies born to obese mothers increases gut permeability and myeloid cell adaptations that provoke obesity and NAFLD. Microb. Cell 6:102–104.
Sun, W., R. Xu, W. Hu, J. Jin, H. A. Crellin, J. Bielawski, Z. M. Szulc, B. H. Thiers, L. M. Obeid, and C. Mao. 2008. Upregulation of the human alkaline ceramidase 1 and acid ceramidase mediates calcium-induced differentiation of epidermal keratinocytes. J. Invest. Dermatol. 128:389–397.
Terragni, R., A. Casadei Gardini, S. Sabattini, G. Bettini, D. Amadori, C. Talamonti, M. Vignoli, L. Capelli, J. H. Saunders, M. Ricci, and P. Ulivi. 2014. EGFR, HER-2 and KRAS in canine gastric epithelial tumors: a potential human model? PLoS One 9:e85388.
Wahlström, A. 2019. Outside the liver box: the gut microbiota as pivotal modulator of liver diseases. Biochim. Biophys. Acta Mol. Basis Dis. 1865:912–919.
Xin, D., L. Zong-Shun, W. Bang-Mao, and Z. Lu. 2014. Expression of intestinal tight junction proteins in patients with non-alcoholic fatty liver disease. Hepatogastroenterology 61:136–140.